ChemComm

COMMUNICATION

View Article Online
View Journal | View Issue

Cite this: *Chem. Commun.*, 2026, **62**, 4570

Received 27th November 2025,
Accepted 20th January 2026

DOI: 10.1039/d5cc06701d

rsc.li/chemcomm

Cooperative organic alloy nanoparticles built from a matching pair of quadrupolar dyes showing unusual fluorescence behaviour

Eleonore Kurek,[a] Pietro Mancini,[b] Jean-Baptiste Verlhac,[a] Benedetta Carlotti*[b] and Mireille Blanchard-Desce*[a]

Binary dye-based fluorescent organic nanoparticles, composed of varying proportions of A and D – two structurally related quadrupolar dyes – exhibit ultrafast and remarkably efficient excitation energy transfer, which in addition promotes fluorescence tuning and quantum yield enhancement as the acceptor content decreases.

Among fluorescent probes for bioimaging, nanoparticles based on organic dyes have become increasingly popular tools, as their high dye content makes them much brighter and more photostable than individual molecular fluorescent probes. In recent years, the incorporation of two or more different dyes, capable of engaging in Förster resonance energy transfer (FRET), has also gained significant attention. Dye-doped polymer nanoparticles are especially popular for intra-particle FRET.[1,2] The polymer matrix may be optically inactive, serving only as a nanocarrier for the molecular donor and acceptor, or, in the case of conjugated polymers, it can itself act as the FRET donor.[1] Dye-doped silica-based nanoparticles have likewise shown very promising applications.[3,4] The role of FRET varies widely across different systems. It can be employed to obtain colour-tunable particles by adjusting the donor and acceptor ratios and their respective emission intensities, as well as through sequential FRET involving more than two dye types.[5,6] The donor can also function as an energy antenna, enabling efficient light harvesting,[7] including multiphoton harvesting, which allows for the effective excitation of acceptors with poor two-photon absorption cross sections.[4,8] Furthermore, in the case of small-molecule ionic isolation lattices (SMILES), adding an acceptor enhances the optical properties of the material, by having FRET outcompete energy migration to the quenching sites.[9]

Recently, we showed that self-stabilized dye-based fluorescent organic nanoparticles (dFONs) made from polar and polarizable dyes (PPD) represent an innovative approach towards ultra-bright probes for bioimaging applications. Such dFONs show good structural and colloidal properties, thanks to the nature of their building blocks.[10] Moreover, modifying the structure and geometry of the PPD is an effective way to bottom-up engineer the optical properties and surface properties of dFONs: they can be rendered stealth[11] or alternatively made to internalize within cells.[12] Another salient structural characteristic of dFONs made from PPDs is that high surface potentials can be achieved, promoting excellent colloidal stability[11–13] and efficacious cooperative electrostatic interaction-promoted surface coating.[12] This characteristic also allows the formation of entirely dye-based core–shell nanoparticles using a sequential nanoprecipitation procedure.[14,15] Such binary dFONs (BFONs), made from complementary dipolar dyes, show efficient shell-to-core energy transfer[14,15] and an unprecedented enhancement of the FRET-mediated fluorescence quantum yield of the acceptor (by a factor of up to 20).[15] Yet only indirect excitation of the acceptor leads to the fluorescence quantum yield enhancement of acceptor (core) emission. In order to overcome this limitation, we turned to alloy-type dFONs made from quadrupolar dyes. We selected D (energy donor) and A (energy acceptor) (Fig. 1a) – a pair of optically complementary quadrupolar chromophores[12] that share a similar structure built around one benzothiadiazole electron-withdrawing core and two diphenylamine electron-releasing moieties at their extremities. In A, the π-bridge is extended by the addition of thienyl units, thus considerably red-shifting its absorption and emission compared to D. This shift is preserved upon nanoprecipitation (Fig. 1b), where D and A yield stable suspensions of orange-emitting DdFONs and near-infrared (NIR) emitting AdFONs, respectively. The significant overlap between the emission spectrum of DdFONs and the absorption spectrum of AdFONs makes them a good FRET pair, with a theoretical Förster radius of 3.6 nm for a single D–A pair. Furthermore, thanks to the bulky fluorenyl and diphenylamino motifs that hinder π-stacking and aggregation caused quenching (ACQ), DdFONs retain substantial fluorescence quantum yield values

[a] *Université de Bordeaux, CNRS, Bordeaux INP, ISM (UMR5255), 351 Cours de la Libération, 33405, Talence, France. E-mail: mireille.blanchard-desce@u-bordeaux.fr*

[b] *Department of Chemistry, Biology and Biotechnology and CEMIN, University of Perugia, 06123, Perugia, Italy. E-mail: benedetta.carlotti@unipg.it*

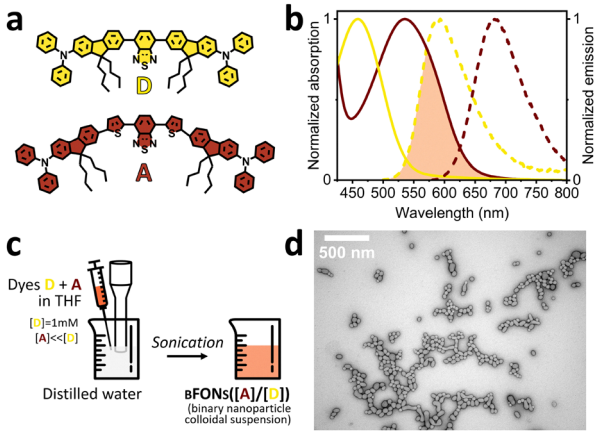

Fig. 1 (a) Molecular structures of dyes D (energy donor) and A (energy acceptor). (b) Absorption (full lines) and fluorescence spectra (dashed lines) of aqueous suspensions of DdFONs in yellow and AdFONs in dark red. Orange: overlap between the fluorescence spectrum of DdFONs and the absorption spectrum of AdFONs, where excitation energy transfer is possible. (c) Preparation scheme of BFONs (binary dFONs). (d) Transmission electron microscopy (TEM) image of BFONs (0.05/1).

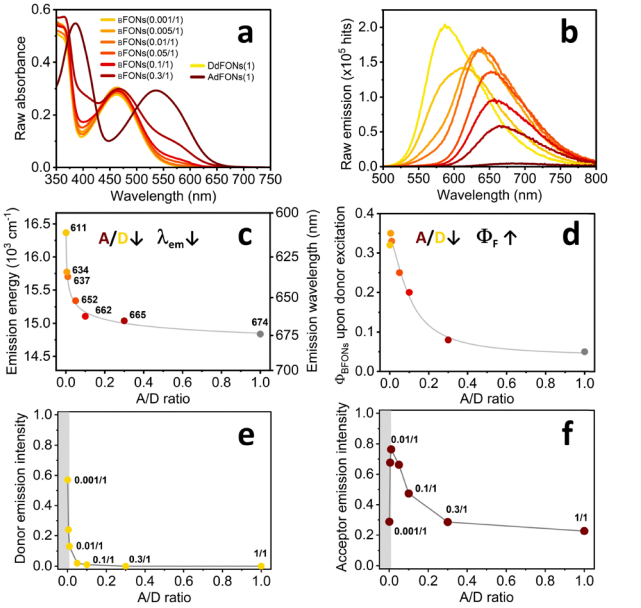

Fig. 2 (a) Raw absorbance spectra of dFON and BFON suspensions. (b) Raw emission spectra of dFON and BFON suspensions upon donor excitation at 445 nm. Fluorescence spectra were acquired on 3-times diluted suspensions under the strict same experimental conditions, so that fluorescence intensities could be directly compared. (c) Maximum emission wavelength (right axis) and corresponding energy (left axis) of BFONs upon donor excitation at 445 nm. (d) Fluorescence quantum yield Φ_{BFONs} of the BFONs upon donor excitation at 445 nm. Grey line: guide for the eye. (e) Donor emission intensity of the BFONs as a function of the A/D ratio (normalized by the emission intensity of DdFONs(1)). The abrupt change in the grey region is attributed to a high likelihood of forming DdFONs in this low A/D ratio domain. (f) Acceptor emission intensity of BFONs as a function of the A/D ratio (normalized by the emission intensity of DdFONs(1)). We attribute the abrupt change in the grey region to a high likelihood of forming DdFONs in this low A/D ratio domain.

in water ($\Phi = 0.30 \pm 0.05$), thus leading to large brightness values ($B = 1.1\ 10^7\ M^{-1}\ cm^{-1}$), while AdFONs show much lower Φ values but emit in the NIR1 region (Fig. 1b).[12]

A series of binary dFONs (BFONs) with decreasing A/D ratios were prepared by nanoprecipitation (Fig. 1c). All BFONs were prepared from stock solutions containing [D] = 1 mM and 0.001 mM < [A] < 0.3 mM in tetrahydrofuran (THF), so that the quantity of donor D remained the same, while varying the quantity of acceptor A. The resulting colloidal BFON suspensions are named BFONs ([A]/[D]), in reference to the stock solution concentrations used. Transmission electron microscopy (TEM) was performed, showing that BFONs appear for the most part spherical, with some ellipsoidal shapes as well (Fig. 1d). The dry diameters measured from the TEM images are represented as size distributions in Fig. S1a–f, and median values are indicated in Table S1. Interestingly, while BFONs (0.01/1), BFONs (0.05/1), BFONs (0.1/1) and BFONs (0.3/1) yield broad distributions centering around 35–40 nm (as illustrated in Fig. S1c–f), the BFONs with the smallest A/D ratio – namely BFONs(0.005/1) and BFONs(0.001/1) – yield bimodal distributions, with one major peak around 11 nm, and a second, very minor peak around 35–40 nm (Fig. S1a and b). The raw absorbance spectra of the resulting BFONs, represented in Fig. 2a, are simply a weighted sum of DdFONs and AdFONs, in accordance with their A/D ratios. However, upon excitation of the donor at 445 nm, the emissive properties of BFONs are found to differ drastically from those of DdFONs and AdFONs.

Indeed, Fig. 2b clearly shows energy transfer from D to A in all BFONs, regardless of A/D ratio, as evidenced by the quenching of donor emission and the appearance of acceptor emission. BFON emission spectra are found to differ in shape, maxima and intensity, depending on their A/D ratio (Fig. 2b), with the emission maxima ranging from 665 nm to 611 nm (Fig. 2c) and fluorescence quantum yields ranging from 0.08 to 0.32 (Fig. 2d) for BFONs (0.3/1) to BFONs (0.001/1), respectively. Detailed photophysical data are summarized in Table S2. In order to analyse these results, a deconvolution of the emission spectra of BFONs was performed, as those with small A/D ratios clearly contain different contributions. Deconvolution of the emission spectra into donor and acceptor contributions (Fig. S2, Table S3) confirms an increase in donor emission as the A/D ratio decreases, from under 1% donor contribution in BFONs (0.3/1) up to 83% in BFONs (0.001/1). These residual donor emission intensities (Fig. S3a) were used to assess FRET efficiencies, resulting in values of up to 99.7% for BFONs (0.3/1) and down to 43% for BFONs (0.001/1) (Table S3). We then used a Stern–Volmer plot to assess our system's energy transfer efficiency (Fig. S3b). The plot shows an upward curvature characteristic for systems where donors and acceptors are confined within small domains, and where statistically, the number of acceptors per domain varies according to a Poisson distribution.[16,17] In our case, this indicates that a certain amount of the observed donor emission likely comes from nanoparticles that contain no acceptors. The probability of forming such DdFONs (1) increases as the A/D ratio and the nanoparticle size decrease (Fig. S3c). The energy transfer efficiencies in BFONs (0.001/1) and BFONs (0.005/1), evaluated using donor

emission intensities, are thus underestimated. Since most models accounting for sample heterogeneity make assumptions that do not apply to our samples (narrow aggregate size or constant fraction of inaccessible donors irrespective of A/D ratio[16]), we instead applied segmented linear fits to the data. This highlighted two main regimes: a low A/D regime (0.001/1–0.01/1), with a shallow slope (663), reflecting the presence of many donor-only aggregates, and a higher A/D regime (0.05/1–0.3/1), where the steeper slope (1093) reflects greater quenching efficiencies. This means that one acceptor roughly quenches 1093 donors, which is a full order of magnitude above the number of dyes that lie within the quenching sphere defined by the Förster radius (115 dyes). This excellent quenching efficiency suggests efficient exciton diffusion within bFONs.[1] Even more intriguing insights can be gained by looking at the behaviour of the acceptor: upon deconvolution, it appears that the initially observed blue shift of the raw bFON emission (Fig. 2b) is not simply due to a contribution of donor emission, but rather comes from a blue shift of the acceptor emission itself (Fig. S5a). We attribute this variation of the acceptor emission towards the A/D ratio to the specific nature of our dyes. Indeed, no such effects were observed by McNeil *et al.* on PFBT polymer nanoparticles doped with perylene red, despite the donor properties being very similar to our own.[18] We posited that environmental polarity could be responsible for this blue shift and we studied the dyes' solvatochromism (Fig. S6) using the Lippert–Mataga relationship[19,20] to estimate the environmental polarity felt by A dyes within bFONs (Fig. S7). We found that the Stokes shift of A in bFONs(1/0.3–0.05/1) corresponds to polarities lying between that of DdFONs ($\Delta f = 0.03$) and AdFONs ($\Delta f = 0.19$), with progressively decreasing polarities matching the observed blue shift for lower A/D ratios. In addition, whereas previous literature on statistically mixed binary systems overwhelmingly shows a decrease in acceptor intensity upon decreasing the A/D ratio (Fig. S8),[7,17] our system shows the opposite: for A/D ratios up to and including 0.01/1, the emission intensity increased (Fig. 2f). Thus, we attribute the increase in acceptor fluorescence intensity with decreasing A/D ratios to an enhancement of the fluorescence quantum yield of the acceptor itself. To the best of our knowledge, such an effect has only been observed once before by Ishow *et al.*[21] We note striking similarities between this environmental emission enhancement (EEE) effect in bFONs with A/D < 0.3 and the previously reported nanointerfacial emission enhancement (NIEE) effect in core–shell nanoparticles.[22] These new results suggest that no such donor–acceptor nano-interface is necessary for acceptor enhancement, as long as acceptors are exposed to a majority-donor environment. Dividing the fluorescence quantum yield of such binary systems by that of the corresponding pure acceptor AdFONs yields the EEE factor. In this paper, we report a maximum EEE value of 12 (Table S2) for bFONs (0.005/1). While the maximum reported NIEE factor for core–shell nanoparticles – 20 for D/A = 1/1[15] – remains higher, we were able to obtain a similar magnitude of emission enhancement using 200 times less acceptor here. Thanks to efficient EEE, ultimate nanoparticle brightness values of 9×10^7 M^{-1} cm^{-1} were obtained for bFONs (0.05/1) emitting in the deep red (652 nm). As such, they are among the brightest reported red-emitting organic nanoprobes,[23] a full order of magnitude above quantum dots QD655 (4×10^6 M^{-1} cm^{-1} per particle).[11] Next, we performed femtosecond transient absorption and fluorescence upconversion experiments to gain more insights into excited state and fluorescence emission dynamics. The broadband fluorescence up conversion measurements revealed a significant red shift in time of the emission spectra for the DdFONs, with such temporal evolution being less pronounced for the AdFONs (Fig. 3). The time-resolved emission spectra underwent a larger dynamic Stokes shift for dye D compared to A (Fig. S9 and S10). This is consistent with the observed steady-state fluorosolvatochromism of dyes D and A (Fig. S6 and S7), in line with symmetry breaking.[24,25] Indeed, the ultrafast spectroscopic investigation performed in solvents of different polarity uncovered the population dynamics from a locally excited ($S_{1,LE}$) to an intramolecular charge transfer state ($S_{1,ICT}$) for these two quadrupolar dyes (Fig. S9–S12 and Table S5),[26,27] which occurs

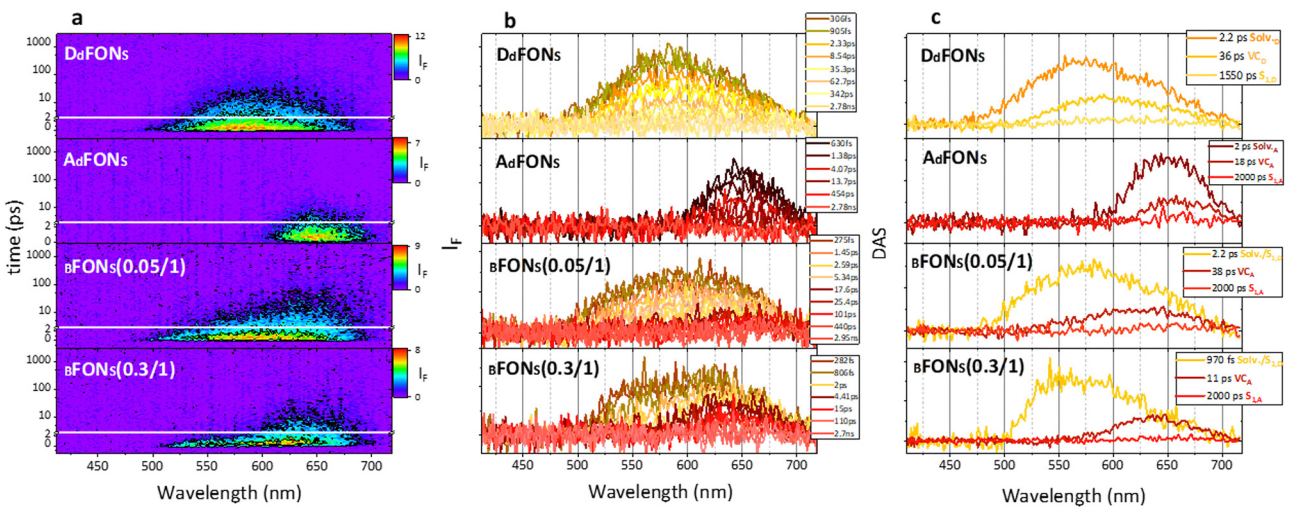

Fig. 3 Femtosecond broadband fluorescence up-conversion spectroscopy of aqueous suspensions of DdFONs, AdFONs, bFONs (0.05/1) and bFONs (0.3/1): (a) 3D data matrices, (b) time-resolved emission spectra and (c) decay-associated spectra obtained from global analysis.

within a few picoseconds together with solvation and becomes faster upon increasing the solvent polarity. The time resolved absorption and emission spectra obtained for the pure DdFONs and AdFONs exhibited distinct and characteristic features. In the case of the pure donor organic nanoparticles, the time resolved emission spectra peaked between 550 and 600 nm (Fig. 3), while the transient absorption spectra showed negative ground state bleaching signals below 500 nm and a pronounced positive excited state absorption above 620 nm (Fig. S13). Such spectral features closely resemble those observed for the D dye in toluene (Fig. S9 and S11), in agreement with the low environmental polarity felt by the DdFONs (Δf = 0.03). In the case of the pure acceptor organic nanoparticles, the time resolved emission spectra peaked around 650 nm (Fig. 3), while the transient absorption spectra exhibited a pronounced ground state bleaching at *ca.* 540 nm (Fig. S13). When BFONs with 0.05/1 and 0.3/1 ratios were considered, the time resolved emission spectra recorded upon preferential donor excitation at 400 nm show a significant temporal evolution (Fig. 3). At early delays after photoexcitation, the emission spectra are centred at 550–570 nm in the donor emission region. Interestingly, at longer time delays, the fluorescence spectra are peaked at *ca.* 640 nm in correspondence with the acceptor fluorescence. Such spectral evolution suggests the occurrence of FRET in the BFONs.[28,29] This was confirmed by the femtosecond transient absorption results obtained for the BFONs (Fig. S13). The early transient spectra show ground state bleaching below 500 nm and excited state absorption above 620 nm, resembling the spectral features of excited DdFONs. Differently, the late transient spectra are characterized by a negative signal around 560 nm, which may be due to the acceptor ground state bleaching. The results of the global analysis of these data for the pure donor and acceptor nanoparticles as well as for the BFONs are detailed in graphs c of Fig. 3 and Fig. S13 and in Table S6. The lifetime associated with the quenched donor in the binary nanoparticles and thus with the energy transfer process was found to be *ca.* 2 ps for the (0.05/1) and *ca.* 0.95 ps for the (0.3/1) BFONs, respectively. It is noteworthy that the FRET time decreases upon increasing the acceptor amount in the binary nanoparticles. Interestingly, considering these τ_{DA} lifetimes together with the τ_D lifetime of *ca.* 2000 ps for the donor nanoparticles in the absence of acceptor (Table S6), the FRET efficiency ($E = 1 - \tau_{DA}/\tau_D$) can be estimated to be *ca.* 99.9% in our experimental conditions. In summary, our femtosecond spectroscopic results confirm ultrafast and quantitative exciton diffusion from the donor to the acceptor dyes within the investigated binary alloy nanoparticles.

Conflicts of interest

The authors declare no conflicts of interest.

Data availability

The data supporting this article have been included in the supplementary information. Additional details can be obtained from the authors upon request.

Supplementary information (SI) is available. See DOI: https://doi.org/10.1039/d5cc06701d.

Acknowledgements

The authors thank the University of Bordeaux for a fellowship to E.K. The authors acknowledge the support from the LIGHT S&T Graduate Program of Bordeaux (PIA3 Investment for the Future Program, ANR-17-EURE-0027). Electronic microscopy was performed at the Bordeaux Imaging Center, a service unit of the CNRS-INSERM and Bordeaux University, member of the national infrastructure France BioImaging supported by the French National Research Agency (ANR-10-INBS-04). The help of Sabrina Lacomme is acknowledged for technical assistance in electron microscopy. The authors also acknowledge financial support by the European Union under the Italian Ministry of University and Research (MUR) National Innovation Ecosystem grant ECS00000041 – VITALITY and by the MUR under the PRIN 2022 program (No. 2022RRFJC4).

References

1 Y. Jiang and J. McNeill, *Chem. Rev.*, 2017, **117**, 838–859.
2 A. Reisch and A. S. Klymchenko, *Small*, 2016, **12**, 1968–1992.
3 D. Genovese, E. Rampazzo, S. Bonacchi, M. Montalti, N. Zaccheroni and L. Prodi, *Nanoscale*, 2014, **6**, 3022–3036.
4 N. Bondon, C. Charlot, L. M. A. Ali, A. Barras, N. Richy, D. Durand, Y. Molard, G. Taupier, E. Oliviero, M. Gary-Bobo, F. Paul, S. Szunerits, N. Bettache, J.-O. Durand, C. Nguyen, R. Boukherroub, O. Mongin and C. Charnay, *J. Mater. Chem. B*, 2025, **13**, 1767–1780.
5 L. Wang and W. Tan, *Nano Lett.*, 2006, **6**, 84–88.
6 A. Wagh, F. Jyoti, S. Mallik, S. Qian, E. Leclerc and B. Law, *Small*, 2013, **9**, 2129–2139.
7 K. Trofymchuk, A. Reisch, P. Didier, F. Fras, P. Gilliot, Y. Mely and A. S. Klymchenko, *Nat. Photonics*, 2017, **11**, 657–663.
8 Z. Xu, Q. Liao, X. Shi, H. Li, H. Zhang and H. Fu, *J. Mater. Chem. B*, 2013, **1**, 6035.
9 L. Kacenauskaite, S. G. Stenspil, A. H. Olsson, A. H. Flood and B. W. Laursen, *J. Am. Chem. Soc.*, 2022, **144**, 19981–19989.
10 J. Daniel, O. Dal Pra, E. Kurek, C. Grazon and M. Blanchard-Desce, *C. R. Chim.*, 2024, **27**, 1–17.
11 M. Rosendale, J. Flores, C. Paviolo, P. Pagano, J. Daniel, J. Ferreira, J. Verlhac, L. Groc, L. Cognet and M. Blanchard-Desce, *Adv. Mater.*, 2021, **33**, 2006644.
12 P. Pagano, M. Rosendale, J. Daniel, J.-B. Verlhac and M. Blanchard-Desce, *J. Phys. Chem. C*, 2021, **125**, 25695–25705.
13 J. Daniel, F. Bondu, F. Adamietz, M. Blanchard-Desce and V. Rodriguez, *ACS Photonics*, 2015, **2**, 1209–1216.
14 E. Campioli, C. Rouxel, M. Campanini, L. Nasi, M. Blanchard-Desce and F. Terenziani, *Small*, 2013, **9**, 1982–1988.
15 C. Mastrodonato, P. Pagano, J. Daniel, M. Vaultier and M. Blanchard-Desce, *Molecules*, 2016, **21**, 1227.
16 M. H. Gehlen, *J. Photochem. Photobiol., C*, 2020, **42**, 100338.
17 C. Wu, H. Peng, Y. Jiang and J. McNeill, *J. Phys. Chem. B*, 2006, **110**, 14148–14154.
18 L. C. Groff, X. Wang and J. D. McNeill, *J. Phys. Chem. C*, 2013, **117**, 25748–25755.
19 E. Lippert, *Z. Naturforsch., A: Phys. Sci.*, 1955, **10**, 541–545.
20 N. Mataga, Y. Kaifu and M. Koizumi, *Bull. Chem. Soc. Jpn.*, 1956, **29**, 465–470.
21 S. Hoang, S. Olivier, S. Cuenot, A. Montillet, J. Bellettre and E. Ishow, *ChemPhysChem*, 2020, **21**, 2502–2515.
22 E. Kurek, M. Rosendale, G. Recher, J.-B. Verlhac, S. Marais, J. Daniel and M. Blanchard-Desce, *Chem. – Eur. J.*, 2025, e01698.
23 A. H. Ashoka, I. O. Aparin, A. Reisch and A. S. Klymchenko, *Chem. Soc. Rev.*, 2023, **52**, 4525–4548.
24 M. Söderberg, B. Dereka, A. Marrocchi, B. Carlotti and E. Vauthey, *J. Phys. Chem. Lett.*, 2019, **10**, 2944–2948.

25 F. Terenziani, A. Painelli, C. Katan, M. Charlot and M. Blanchard-Desce, *J. Am. Chem. Soc.*, 2006, **128**, 15742–15755.
26 Y. Rout, C. Montanari, E. Pasciucco, R. Misra and B. Carlotti, *J. Am. Chem. Soc.*, 2021, **143**, 9933–9943.
27 F. Ricci, F. Elisei, P. Foggi, A. Marrocchi, A. Spalletti and B. Carlotti, *J. Phys. Chem. C*, 2016, **120**, 23726–23739.
28 M. Alebardi, C. Munzone, E. Sorbelli, A. Grasso, L. Mencaroni, F. Elisei, C. G. Fortuna, A. Spalletti, C. Bonaccorso and B. Carlotti, *Adv. Funct. Mater.*, 2024, **34**, 2403706.
29 E. L. Taylor, K. J. Metcalf, B. Carlotti, C.-T. Lai, J. A. Modica, G. C. Schatz, M. Mrksich and T. I. Goodson, *J. Am. Chem. Soc.*, 2018, **140**, 15731–15743.

